J. Fluid Mech. (1992), *vol.* 237, *pp.* 541–568
Printed in Great Britain

The interface between fluid-like and solid-like behaviour in two-dimensional granular flows

By YI ZHANG AND CHARLES S. CAMPBELL
Department of Mechanical Engineering, University of Southern California, Los Angeles, CA 90089-1453, USA

(Received 2 January 1990 and in revised form 20 September 1991)

The effective phase change from fluid behaviour to solid behaviour, that too often occurs in granular flow and brings with it such unwelcome events as funnel flows in hoppers and clogging of other material handling devices, is studied using a discrete particle computer simulation of a Couette flow with gravity. This simulation exhibits the full range of granular flow behaviour, from a stagnant solid-like material, through a quasi-static transition zone, to a rapid granular flow. The most important result is that the first movement in the material just above the static bed occurs in a quasi-static mode at a fixed value of the stress ratio τ_{xy}/τ_{yy}. Thus, it appears that the primary transition from solid to fluid behaviour is a yield-like phenomenon and can be described by a Mohr–Coulomb-type failure criterion.

1. Introduction

One of the most intriguing aspects of granular flow is that a granular material may act as either a fluid or a solid. For example, the sand on a beach will easily support a person's weight, but a handful of the same sand will easily flow out between his fingers. Moreover, under many circumstances, both fluid-like and solid-like behaviour may occur simultaneously and meet at an interface within the material. This interface forms a boundary to the flowing material, and this boundary has the special property that its location is determined solely by flow conditions. This study is an attempt to understand the nature of the transition between fluid and solid behaviour by studying the conditions at such an interface.

The state exhibited by a granular material depends on the local stress conditions. When a granular material is showing solid behaviour, much of the load is supported across frictional bonds between the particles and the system's strength is limited to the loads those bonds can support. When enough of the bonds have been overcome, the system will fail and begin to flow. The initial failure will consist of many-particle blocks moving relative to one another along shear bands that roughly follow stress characteristics through the material. Initially, particles, will stay in contact and interact frictionally with their neighbours over long periods of time and the failure will continue in this manner as long as the deformation occurs fairly slowly. This is the 'quasi-static' regime of granular flow and has been classically studied using modified plasticity models based on a Mohr–Coulomb failure criterion. However, if the motion is rapid enough, sufficient energy can be transferred to the particles next to the slip lines to break them free of their parent blocks. The slip regions will grow until every particle in the granular mass is moving independent of even its nearest neighbours. Under these conditions (referred to as the 'rapid flow regime'), the particles behave analogously to molecules in the kinetic theory of gases. In fact,

transport processes are assumed to be governed by a field quantity called the 'granular temperature' which is defined as the kinetic energy per unit mass contained in the random motions of the particles, and is, in most ways, equivalent to the thermodynamic temperature of a gas. Such systems are generally modelled using techniques borrowed from kinetic theory. (A recent review of the rapid flow regime can be found in Campbell 1990.) All three conditions – the stagnant, the quasi-static and the rapid – may occur in the transition from solid-like to fluid-like behaviour.

Some of the most interesting cases of the solid/fluid transition are encountered when both conditions coexist and meet at an interface located somewhere within the material. Natural examples include large-scale ground failures (where portions of a granular material will yield and flow while the bounding regions remain stationary), the bottom boundaries of landslides, and the onset of motion in stream beds and slurry flows (although fluid forces will be important for most examples of these last two cases). The greatest problems of this type arise in industrial situations, where undesired stagnant zones form in material handling devices. Usually, this occurs because the material cannot follow the prescribed flow path set out by the boundaries of the apparatus and a portion of the material may solidify to create a more favourable channel shape. This is undesirable in devices primarily designed for bulk material transportation as the particle mass blocks the flow passage and causes a severe reduction in, if not a complete halting of, the mass flow. To prevent the stagnant zone formation, walls are mechanically shaken, the material is stirred or air is injected to partially fluidize the material. Even then the problem is often solved in a most practical manner by some 'judicious pounding at points where stoppages occur' (Wolf & von Hohenleiten 1945).

Probably the most extensively studied industrial system is a hopper. There, stagnant zones form along the converging walls of the hopper and produce a condition known as 'funnel flow', so called because the stagnant material forms a funnel-like boundary to the flowing region. The stationary material lies along the bottom of the hopper and it will stay there until the hopper is emptied and cleaned – which, for industrial hoppers in continuous use, may not occur for several years. Thus, in many cases, the prevention of funnel flow is a more important design criterion than the flow rate that can be obtained from the hopper. (For other cases, however, funnel flow may be desirable. For example, it has long been known that roughening the walls of hoppers paradoxically increases the mass flow rate. Nguyen (1979) explained this phenomenon by showing that the roughened walls force a flow transition from a fully flowing state to funnel flow and that the channel formed by the funnel, having a steeper inclination than the hopper walls, results in the improved mass flow rate.)

Thus, one of the most important and yet still lacking requirements in the handling of particulate solids is a set of criteria that a design engineer can use to predict and prevent the formation of stagnant zones within what should be freely flowing material. This mirrors the more basic problem of defining appropriate boundary conditions for theoretical analyses of granular flow (which is difficult enough, even if one does not have to be concerned about a phase change). The only attempt to handle the effective phase-change problem is a recent analysis by Jenkins & Askari (1991). They used the analogy between rapid flow behaviour and the kinetic theory of gases and assumed that the material transitions directly from a rapid flow state to a solid state, with the transition governed by some sort of P–V–T criterion similar to that obeyed by a normal thermodynamic material. While, on one level, this seems

reasonable, it may well be taking the analogy between rapid granular flows and gases too literally. In particular, granular materials may still exhibit fluid-like behaviour while undergoing quasi-static motion for which the above ideas are invalid. In general, much more needs to be known about the nature of the boundaries that form between the flowing and stagnant regions of granular flows to guide both engineering understanding and future theoretical developments.

A preliminary report of this work may be found in Zhang & Campbell (1990).

2. Computer simulation

The problem is studied using a discrete-particle computer simulation, a method proven to be an invaluable technique for studying dense particle flows as everything is known about the simulated system and all the details of the flow are accessible to the computer 'experimenter'. We chose a soft-particle model for this study (for a discussion of the various computer modelling techniques, see the review by Campbell 1986*a*) which, while it may be the most computationally inefficient method for modelling granular flows, it is the only exact method that can accurately model flows containing stagnant regions with their long-duration contacts between particles. As the modelling technique is fairly standard, it will be given only the most cursory treatment here. For more details, the reader is referred to Campbell & Zhang (1989).

With current computers, it is impossible to build a computer model for the millions or billions of particles that would exist in even a laboratory-scale apparatus. The best one can do is to choose a system that preserves as many features of the flow as possible, but can hopefully be studied with less than 1000 particles. At first it may seem like a stretch of the imagination to think that such a small system can accurately reflect the features of a funnel flow in a hopper, but actually, near the interface, the hopper flow is quite simple. There, stress is applied to the interface by the flowing material in the central core of the hopper, while, in addition, a gravitational body force acts to pull the particles vertically downward. (The effect of gravity is somewhat complex in that, in one direction, it provides the motive force for the flow, but, in another, holds the material against the walls of the hopper against which the frictional response halts the flow and causes the stagnant regions to form.) With this picture in mind, an appropriate situation to model would be a Couette flow with a gravitational acceleration vector oriented perpendicular to the flow direction, such as that shown schematically in figure 1. The purpose of the walls is simply to drive the flow and to impose a stress state on the material while confining the particles in the vertical direction; hopefully, the walls would impose no further constraint on the flow and we found this to be true in all but a few cases. Here, the sole purpose of the gravity vector is to force a phase-change interface to occur somewhere between the walls.

The computer simulation is performed on the two-dimensional rectangular control volume illustrated in figure 1. The bottom of the control volume is bounded by a stationary solid wall while the top is bounded by another wall which moves in response to applied forces. The movement of the top wall is determined by balancing an externally applied horizontal force per unit area, X, and a vertical force per unit area, Y, with the reaction forces generated internal to the material. The force Y represents the weight of the top wall, Mg/L, where M is the mass of the wall and L is the width of the control volume. The wall accelerates until the forces generated within the granular material balance the forces applied to the wall. Once the velocity of the top wall has converged to a nearly constant value, the stress state at the top

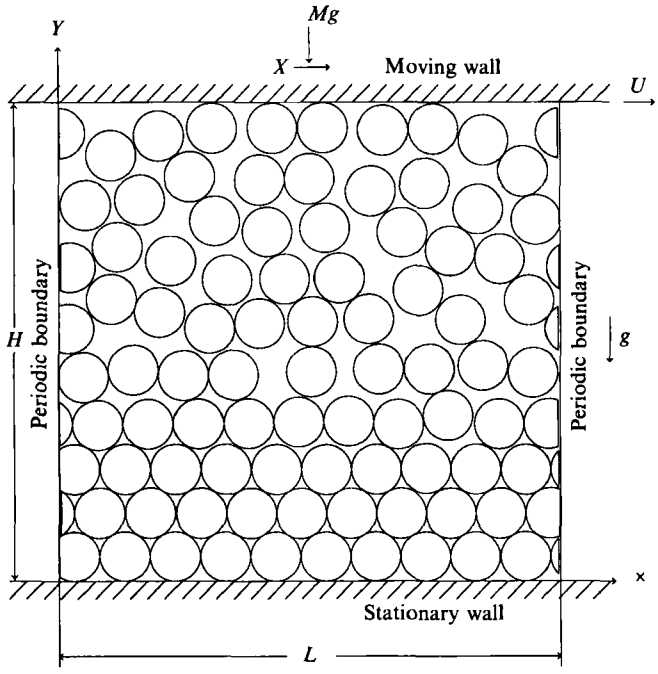

FIGURE 1. Schematic of the simulation control volume. A Couette flow with gravity is modelled. The flow is driven by the forces, X and Y, applied to an upper moving boundary and restrained by a lower stationary boundary. A gravitational body force causes the material to assume solid behaviour near the bottom wall.

wall of the control volume is fixed to $\tau_{xy} = X$ and $\tau_{yy} = Y$. As there is no acceleration of the material and no additional forces in the x-direction, τ_{xy} must be uniform across the control volume and equal to X everywhere. However, as gravity works in the y-direction, τ_{yy} must vary hydrostatically from the value Y applied at the top of the channel to accommodate the weight of the material. The other two stresses, τ_{xx} and τ_{yx} are self-equilibrated and cannot be specified at a horizontal boundary; the values they assume are determined by the stress reaction of the granular mass to the forces applied at the wall.

Initially, we used a slightly different boundary condition at the top wall, in which we imposed the horizontal velocity of the top wall rather than the horizontal shear stress. However, we found that the velocity of a particle in the neighbourhood of the wall was usually less than the top-wall velocity. Thus, changing the top wall velocity did not directly change the velocity of the flow, but, instead, it varied it indirectly, by changing the stress state in the material. Thus, we altered the upper wall boundary condition as described above, and now directly specify the local stress of the system.

In the direction of flow, the sides of the control volume are bounded by the periodic boundaries. This means that, as a particle passes through such a boundary, it re-enters on the opposite side with exactly the same position along the boundary and velocity with which it left. This type of boundary emulates a situation in which the entire control volume is periodically repeated infinitely many times, upstream and downstream, and is a means to model an infinitely long system with a small number of particles. It has the drawback, however, that it is only applicable to flows with no gradients in the flow direction. This constraint was one of the reasons for choosing

a Couette flow with gravity for this study; this geometry naturally has no gradients in the direction of flow and, consequently, permits the use of periodic boundaries, thus reducing the number of particles and necessary computer time, while retaining most of the features of interest of the systems.

Once the shear and normal forces applied to the top wall are specified, the simulation is left to progress as it will until it converges to a statistically stationary condition. Steady conditions are determined from examining three parameters: the total kinetic energy of the system, the height of the control volume and the horizontal velocity of the top wall, all three of which assume nearly constant values at steady state. However, the determination of convergence is a little difficult because, like all small thermodynamic systems, these parameters fluctuate slightly, even under statistically steady conditions. Hence, convergence is somewhat subjectively chosen to occur when it appears to the operator that the average values of these quantities are no longer changing. Usually, the converged state is reached after about 1000–1500 collisions per particle. Once a converged state is obtained, the properties of the system are averaged over a specified period of time to determined velocity profiles, stress distributions and other quantities of interest. The averaging period usually covers about 3000 collisions per particle.

As mentioned previously, the simulation is built about a soft-particle model which may be thought of as the simultaneous numerical integration of an equation of motion for each particle in the system. Each motion equation relates the change in a particle's position to its velocity and the forces to which it is subject. The total force on a particle consists of a constant gravitational acceleration and the forces exerted over the points of contact with its immediate neighbours and the bounding walls of the simulation. Thus, much of the integration procedure involves determining when there is contact between particles or between particles and walls. The simulation proceeds in short time steps which may be thought of as the step size of the numerical integration. The particles interact with each other only when they contact, defined as whenever the centres of two particles lie less than a particle diameter, $2R$, apart where R is the particle radius. As a search for new or broken contacts must be performed at each time step, contact determination consumes the largest fraction of computational time in this simulation. A contact between particles is modelled by assuming that the colliding particles are connected by a linear spring and a linear dashpot connected in parallel in both the normal and tangential direction to the contact point. (This is the most common scenario used for soft-particle models.) The spring provides the restoring force that tries to push the particles apart and the dashpot provides the energy dissipation that makes the collisions inelastic. In addition, a frictional slider with an associated friction coefficient, μ, is added in series with the tangential-direction spring and dashpot so that there is no tangential slip between the particles as long as the tangential force is smaller than μ times the normal force; if this value is exceeded, the particles slip with a force equal to μ times the normal force. The stiffness coefficient (spring constant), K, the damping coefficient (dashpot constant), D, and the friction coefficient, μ, are the three parameters that characterize the nature of the solid material for these simulations. The viscous-like damping coefficient, D, can be related to the more familiar coefficient of restitution, ϵ, by the formula

$$\frac{D}{(Km)^{\frac{1}{2}}} = -\frac{\sqrt{2}\ln(\epsilon)}{(\pi^2+(\ln\epsilon)^2)^{\frac{1}{2}}}, \tag{1}$$

where m is the particle mass. As it is most commonly used in the literature, the

coefficient of restitution, ϵ, will be used as the measure of the particle inelasticity for the rest of this paper.

The boundary conditions at the top and bottom wall are similar to the Type B boundary condition (Campbell 1982, 1988, 1992; Campbell & Brennen 1985). This was an approximate boundary type, originally used to simulate a no-slip condition. As the Type B boundary was for Campbell's rigid-particle model, the velocity of a particle's centroid assumes the velocity of the wall after a collision, with no change in the rotation rate. No attempt is made to use a more exact model in the current study as the sole purpose of the walls in this study is to drive the flow. The Type B condition was chosen because it produces the strongest possible coupling between a particle and the wall. A problem arises, however, because such instantaneous velocity changes are difficult to manage within the framework of a soft-particle model. As the Type B condition is realized here, the spring stiffness K and the damping coefficient D in the direction normal to the wall are the same as those used in a particle–particle collision. However, in the direction parallel to the wall, only a strong damping force exists, which tends to equalize the velocity of the particle and wall. To exactly model a Type B boundary, the damping coefficient, D_w, should be infinite, but, in practice, $D_w = 2.0m(g/R)^{\frac{1}{2}}$ was found to be sufficient. The tangential force is assumed to be applied on the centre of the particle, so that it exerts no moment on the particle and the particle rotational velocity does not change during a collision with a wall. With no gravity, the results of this simulation agree with the rigid-particle simulations with Type B boundaries given by Campbell & Brennen (1985) and Campbell & Gong (1986).

The total force and moment on a particle are the sum of the contact forces and the gravitational force. The subsequent motion of the particle is governed by Newton's second law which leads to a group of ordinary second-order differential equations for each particle. The motion of the entire granular mass is determined by the simultaneous numerical solution of all the differential equations for all the particles. The equations are solved using a standard fourth-order Adams' predictor-corrector method. By comparing the numerical with the exact solution for the collision of two particles, the time step h of the integration was chosen to be $0.075(m/K)^{\frac{1}{2}}$, which yielded a less than 1% error between the exact and numerical solutions.

The averaging procedure used here is essentially the same as used in earlier simulations (e.g. Campbell 1982, 1988, 1992; Campbell & Brennen 1985; Campbell & Gong 1987) and will not be described in detail here. As before, the control volume is divided into strips. Once the system has become statistically stationary, properties such as the solid fraction ν, velocity u, and rotational velocity ω are averaged inside every strip at intervals of about five hundred time steps (about one collision per particle). The result is the distribution of properties in the direction perpendicular to the direction of the flow. The periodic boundary condition eliminates the possibility of time-averaged spatial variations along the flow direction and, consequently, no such data are gathered. A strip width of slightly more than one particle diameter was chosen since, as will be seen, a great deal occurs over such small lengthscales.

The distribution of stress within the system is a more complicated problem. The forces that are macroscopically described by a stress tensor are reflections of the transport of momentum internal to the material. There are two mechanisms that account for the momentum transport. The first, or streaming mode, denoted $\boldsymbol{\tau}_s$, reflects the momentum that is carried by particles as they move through the bulk material with their random velocity. In both function and appearance, the streaming

stress tensor is exactly the same as the Reynold's stress tensor in turbulent flow:

$$\boldsymbol{\tau}_s = -\rho_p \nu \langle \boldsymbol{u}'\boldsymbol{u}' \rangle, \tag{2}$$

where $\langle \boldsymbol{u}'\boldsymbol{u}' \rangle$ is the average of the dyadic product of the fluctuating velocity vectors, $\boldsymbol{u}'$. Obviously, the magnitude of the streaming stresses should be related in some way to the magnitude of the granular temperature. (Note that $\boldsymbol{\tau}_s$ is necessarily symmetric.) Also, when two particles collide, momentum is transferred from the centre of one particle to the other. This is the collisional mode of momentum transfer and results in the collisional stress tensor, $\boldsymbol{\tau}_c$:

$$\boldsymbol{\tau}_c = 2R\langle \boldsymbol{F}\boldsymbol{k} \rangle, \tag{3}$$

where $\langle \boldsymbol{F}\boldsymbol{k} \rangle$ is the appropriate average of the dyadic product of $\boldsymbol{F}$, the vector force exerted by a contact between particles and $\boldsymbol{k}$, the unit vector connecting the particle centres at the time of collision. This reflects the fact that, in a time step h, every collision causes the transport of momentum $\boldsymbol{F}h$ a distance $2R$ in the $\boldsymbol{k}$ direction, between the particle centres. (Note that, as collisional forces are exerted at the edge of the particle rather than its centre, the possibility exists that the collisional stress tensor, $\boldsymbol{\tau}_c$, may be asymmetric. Indeed, such asymmetries have been observed near solid boundaries by Campbell 1988, 1992 and Campbell & Gong 1987.) Obviously, the collisional mode will be more important at large density where a particle cannot move far between collisions, and the streaming mode is dominant at low densities where collisions are infrequent and particles move a large distance between collisions.

In a macroscopic continuum sense, the transport of angular momentum is independent of the transport of linear momentum even though, on the microscopic level, both result from the same forces applied at the same interparticle contacts. Thus, another field variable, the couple stress tensor, $\boldsymbol{M}$, is required to describe the transport of angular momentum. This is a direct analogue of the Cauchy stress tensor and reflects the transport of angular momentum both by streaming and collisional action. The streaming portion of the couple stress tensor, $\boldsymbol{M}_s$, is given by

$$\boldsymbol{M}_s = -\tfrac{1}{2}\rho_p R^2 \nu \langle \boldsymbol{u}'\boldsymbol{\omega}' \rangle, \tag{4}$$

where $\frac{1}{2}\rho_p R^2$ is the particle moment of inertia per unit volume and $\langle \boldsymbol{u}'\boldsymbol{\omega}' \rangle$ is the average of the dyadic product of the fluctuating linear and angular velocities. Also, in a time step h, each contact causes a transport of angular momentum $R\boldsymbol{F}\times\boldsymbol{k}h$ a distance $2R$ (between the particle centres) in the k direction. Thus, the collisional contribution to the couple stress tensor is given by

$$\boldsymbol{M}_c = 2R^2\langle \boldsymbol{F}\times\boldsymbol{k}\boldsymbol{k} \rangle. \tag{5}$$

The complete couple stress tensor is found by summing the streaming and collisional contributions. Each component, M_{ij}, of the couple stress tensor may be thought of as 'the surface torque component in the i direction exerted on a surface with outward pointing normal unit vector in the j direction.' Performing an angular momentum balance on a control volume in steady flow, one obtains the expression:

$$M_{ij,j} - \epsilon_{ijk}\tau_{jk} = 0. \tag{6}$$

Thus the asymmetry in the stress tensor is balanced by the divergence of the couple stress tensor. In two dimensions, the particles are forced to rotate within the plane and, as in Couette flow all gradients are in the y-direction, this expression becomes:

$$M_{zy,y} - (\tau_{xy} - \tau_{yx}) = 0, \tag{7}$$

where z is the coordinate direction out of the plane of motion. Thus, even though there will be an M_{zx} component generated in the granular mass, it represents self-equilibrated torques and is not dynamically important.

All the results are presented here in dimensionless form. The non-dimensionalization is accomplished using R, g, and the particle density, ρ_p to form characteristic length, mass and timescales. The rotational velocity, granular temperature and stresses are thus presented non-dimensionally as

$$\omega = \omega^*(R/g)^{\frac{1}{2}}, \tag{8}$$

$$T = T^*/(gR), \tag{9}$$

$$\tau = \tau^*(\rho_p gR), \tag{10}$$

$$\boldsymbol{M} = \boldsymbol{M}^*/(\rho_p gR^2). \tag{11}$$

(Here, the starred quantities are dimensional and the unstarred quantities are dimensionless.)

So far, this study has been confined to two-dimensional flows of discs rather than spheres. The generalization of the simulation to three-dimensions is not particularly complicated although the model will be substantially less efficient computationally. Furthermore, experience indicates that most of the important features of three-dimensional sphere flows are preserved in the two-dimensional disk flows. (Compare, for example, the two-dimensional results of Campbell & Gong 1986 with the three-dimensional results of Campbell 1989.)

3. Results

Figure 2 shows the results from the computer simulation, with top-wall shear force, $XR^2/mg = 3.5$, normal force, $YR^2/mg = 7.5$, and material properties, $KR/mg = 5 \times 10^5$, $D/m(g/R)^{\frac{1}{2}} = 70.7$ (which corresponds to a coefficient of restitution, $\epsilon = 0.8$) and friction coefficient, $\mu = 0.5$. A snapshot from the simulation, the distribution of horizontal velocity, $\langle u \rangle$ (scaled here by the top-wall velocity, U), the solid fraction, $\langle \nu \rangle$, the granular temperature, T and the rotational velocity, $\langle \omega \rangle$ are plotted here. The vertical axis represents the vertical coordinate, y, scaled by dividing by the control-volume height, H. About a third of the way up from the bottom, the material experiences a transition from a stagnant region to a rapidly shearing region. The transition is most easily seen by examining the velocity profile shown in figure 2(*b*). The two points nearest the bottom show zero horizontal velocity, indicating that they are experiencing solid behaviour. The third point from the bottom is slightly different from zero indicating the first appearance of fluid-like behaviour. (Remember that the definition of a fluid, as given in most elementary fluid mechanics courses, is of a material that cannot withstand a shear stress. Thus, we define the transition from solid to fluid behaviour to occur at the first sign of motion within the material.) From the fourth point upward, the material appears to experience uniform shearing, indicative of fully fluidized behaviour.

This behaviour is mirrored in the solid fraction profile (figure 2*c*). There it can be seen that the density is large in the region where the material is experiencing solid behaviour and becomes significantly reduced in the region where the material experiences fluid behaviour. Now, the largest density at which uniform-sized two-dimensional discs can be packed corresponds to a solid fraction of about $\nu = 0.91$, in which state, the centres of the particles are arranged in a triangular pattern. This configuration can be clearly observed in the stagnant region near the bottom of the

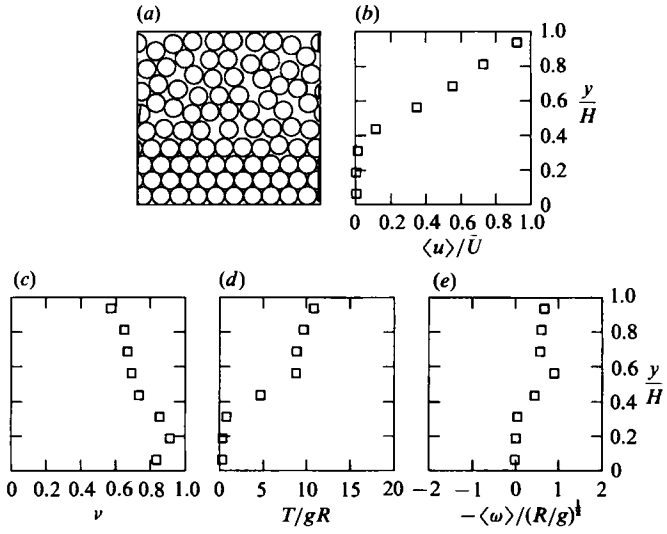

FIGURE 2. Typical results from the simulation, showing (*a*) a snapshot, and (*b*) velocity, (*c*) density, (*d*) granular temperature and (*e*) rotational velocity distributions. Here $XR^2/mg = 3.5$, $YR^2/mg = 7.5$, $KR/mg = 5\times10^5$, $D/m(g/R)^{\frac{1}{2}} = 70.7$ ($\epsilon = 0.8$) and $\mu = 0.5$. Here the final top-wall velocity is $U/(gR)^{\frac{1}{2}} = 11.1$

snapshot (figure 2*a*). However, such a packing cannot be sheared without first dilating to a smaller solid fraction. The smallest packing that can be sheared is approximately $\nu = 0.82$ (see the discussion on packing limits in Campbell 1982), which is approximately the density of the material at the point where movement is first observed.

Figure 2 (*d*) shows the distribution of granular temperature or the energy per unit mass contained in the random motions of the particles. It is worth remembering that, in the field of rapid granular flows, the granular temperature plays exactly the same role in governing transport processes as the thermodynamic temperature plays in the kinetic theory of gases. With this analogy in mind, it is not surprising to see that the granular temperature is large in regions where the material exhibits fluid behaviour and small in the regions where it exhibits solid behaviour. Now, to understand the granular temperature requires understanding the energy flow within a rapidly flowing granular material. Owing to the inelasticity of collisions, the granular temperature, unlike its thermodynamic counterpart, cannot be self-sustaining. Instead, its energy must be transferred down from the energy of the mean flow and eventually converted into thermodynamic heat by the collisional inelasticity. The mechanism that generates granular heat has been identified as shear work – which in this configuration is simply the product of the shear stress and the shear rate – so that a temperature change can only be produced in regions that possess a mean flow velocity gradient. Therefore, in our case, granular heat is only being produced in the fluid-like regions of the flow and, consequently, the temperature is greatest in those regions. In the solid-like regions the temperature is barely noticeable, but non-zero. This is evidence of the conduction of granular heat along its gradients in a manner exactly analogous to the conduction of thermodynamic heat by molecules. By this means, the granular temperature, which is produced in the fluid-like regions, is transported into the solid-like regions of the flow.

This picture suggests that the fluid/solid transition may be governed by some sort

of P–V–T criterion akin to the phase change that occurs in a normal material. Remember that the pressure increases hydrostatically from the top to the bottom of the channel. Hence near the bottom wall the pressure is large and, as the temperature is low, the granular mass adopts a density that is too large to be sheared and the material experiences solid behaviour. Further up, the pressure is reduced, the temperature is higher, and the packing is loose enough that the material can behave like a fluid. Presumably, if enough temperature can be conducted into the solid region to dilate it into a shearable packing, the entire material would experience a fluidized state. (However, as shall be seen, such a conclusion is premature.)

Even so, it is clear from figure 2(*a*) that the initial failure at the interface is not an order–disorder transition where the 'molecules' go from an ordered arrangement in the solid to a disordered state in the fluid region. Instead, the first appearance of fluid behaviour consists of an ordered layer of particles, moving in concert in the direction of flow. This process is reminiscent of the 'layered' microstructure that Campbell & Brennen (1985) observed to form in a granular material at large density. They showed that a two-dimensional granular material could maintain itself in a fluidized state at high concentration by organizing itself internally into layers oriented in the direction of flow. As the particles within a given layer move with the same average velocity, the velocity gradient is maintained by slip between the layers. In effect, this shear-induced microstructure 'pushes through' the phase change by permitting flow at concentrations that would, otherwise, experience solid behaviour. Apparently, the same sort of process accompanies the effective phase change observed in the simulation (which leads to the speculation that the phase-change behaviour might be somewhat different if the flow conditions or the geometry of the control volume did not permit such a microstructure to form). Notice that there is only one perfectly formed layer in figure 2(*a*) (about the fourth row of particles up from the bottom). The next row up is nearly a perfect layer except that there is a large gap near the centre that indicates that one of its constituent particles has been knocked free. Further upward, the organization of the particles becomes progressively more random.

The major consequence of the layered microstructure is its effect on the preferred angles for collisions between particles. Campbell & Brennen (1985) showed that, for uniformly shearing flows at small concentrations, the probability of a collision at an angle (measured relative to the direction of flow) showed an almost sinusoidally varying shear-induced anisotropy. (Similar behaviour was predicted theoretically by Savage & Jeffrey 1981.) The results indicated a preference for collisions in the second and fourth quadrants, reflecting the fact that the velocity gradient tends to promote collisions with the faster moving particles from above and behind, and with the slower moving particles from in front and below. However, at larger densities, when the microstructure has developed, the layers interfere with the angles at which collisions between particles can occur, so that a particle is most likely to collide with particles in its own layer or its immediately neighbouring layers. Collisions with particles in its own layer will centre around the streamline followed by the layer, indicating a preference for collisions near 180°, and the peak that forms across 0° and 360°. Furthermore, the other particles in its layer prohibit collisions with particles in neighbouring layers except in small regions centred around 90° and 270°. Thus, when the layered structure is fully developed, there should be four peaks in the collision angle distribution, located at 90° intervals. Noting that this collisional preference controlled the direction at which force is transmitted internally to the material, Campbell & Brennen were able to associate this microstructure development with an

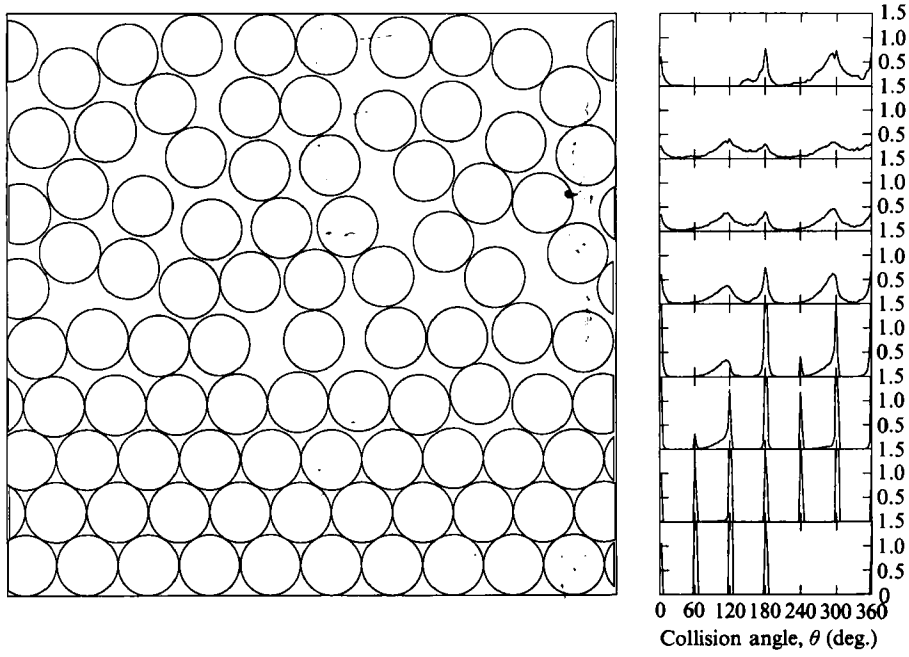

FIGURE 3. The collision angle distribution and its variation across the control volume. The collision angle, θ, is defined as illustrated above. Note that a collision at an angle, θ, for one particle is a collision at an angle $\pi+\theta$ for its partner. Data taken from the same simulation as figure 2.

experimentally observed reduction in the stress ratio, τ_{xy}/τ_{yy}, at large concentrations.

Unlike Campbell & Brennen's simulation, the case studied here is not uniform in either density or shear rate and shows all of the above-mentioned features simultaneously, along with those that would be expected in stagnant regions. The variation in the collision angle distribution is plotted in figure 3. Here, each distribution is compiled for only the collisions whose contact points lie within the appropriate sampling strip. A collision is assumed to occur whenever a contact is made between particles, so that a long-duration contact would only be assessed as a single collision. Thus, this distribution also reflects the activity of the particles as it is revealed in the rate at which contacts are made and broken. In the stagnant regions at the bottom of the channel, the particles are packed with their centres arranged into a triangular configuration. Each particle is in contact with six of its neighbours and the collisions occur in six tightly peaked regions at 60° intervals. (Collisions with the walls are not assessed so that the distribution nearest the bottom wall shows only four peaks, corresponding to contacts between a particle and those in its own layer and in the layer above.) Notice, however, that the largest peaks occur at angles of 120° and 300°. This should be expected as the material experiences a shear force to the right and a normal force downward, so that this is the major direction of force transmission within the material. Going upward through the material, the distribution segues into the four-peaked distribution associated with the layered microstructure, with peaks every 90°. The smooth transition is most apparent in the fourth strip up from the bottom, which in the lower half-disk ($180° < \theta < 360°$) has its contacts distributed every 60° as in the solid phase, and in the upper half-disk ($0° < \theta < 180°$) shows the contacts distributed every 90° as is

characteristic of the layered microstructure. This transition is suggested, in the third strip, by the near disappearance of the peak at 60° and the broadening of the peak at 120° (which eventually becomes the broader peak at 90° in the fourth strip). In turn, the distribution for the fourth strip is almost a mirror image showing a near disappearance of the peak at 240° and a broadening of the peak at 300° (which eventually becomes the peak at 270° for the fifth strip). By the fifth strip, the distribution is showing the behaviour associated with the layered microstructure. In fact, this curve is nearly identical to that measured by Campbell & Brennen (1985) for $\nu = 0.65$ (which is approximately the density in the fifth strip). By the seventh strip, the peaks are nearly gone and the distribution is close to the almost sinusoidally varying shape that Campbell & Brennen associated with low-density shear flows. The peaks reappear in the eighth or highest strip where the particles again form a layer as the material organizes itself to adopt the shape of the top wall.

Returning to figure 2, the final plot (*e*) is the rotational velocity distribution. In the stagnant region, particles have no rotation, but, as the material starts to shear, the rotational velocity becomes non-zero in the transition region (fourth and fifth layer). The computer simulation of Campbell & Gong (1986) shows that the ratio of the average rotational velocity to the shear rate is approximately $-\frac{1}{2}$ in a uniformly shearing flow. Campbell (1988, 1992) and Campbell & Gong (1987) have also shown that large rotations are possible at boundaries but the effect is local and, far from the boundary, the rotation returns to $-\frac{1}{2}$ the shear rate. Exactly this behaviour is apparent in figure 2. One might think of the effective phase change as a boundary on the flowing region and, at this boundary, a large rotation rate is generated as a layer of particles rolls over the stagnant layer beneath it. But notice that the largest degree of rolling occurs not for the first strip in the fluid-like region, but in the strip directly above it. In contrast, Campbell & Gong (1987) studied the effects of a boundary consisting of a densely packed layer of particles glued to a solid wall and found that the wall induced the largest rotation to the particles located right next to the boundary. This is identical to the boundary shape that the stagnant zone presents to the particles in the first flowing layer, yet, in this case, the largest rotational velocity is not seen directly on the boundary. The difference must be attributed to something in the nature of the phase-change surface and can be understood by carefully considering the effects of the layered configuration that exists in the material just at the point of yield. In the fourth strip, the material is barely shearing and the particles are tightly arranged as a layer and, so, interact strongly with their neighbours. Both the movement of the layer over the stagnant zone beneath it and collision with faster moving particles above tend to make the particles in that first moving layer try to roll with a clockwise rotational velocity. However, a collision between two particles with the same sense of rotation – and all other velocities equal – will apply an impulse that tends to work against the rotation of both particles. Hence, the particles in a layer will be prevented from rotating their neighbours in the same layer. Therefore, this first moving layer is more sliding than rolling over the stagnant layer below. Exactly this type of behaviour was apparent in the results of Campbell & Gong (1986) who showed that the particle rotation disappeared at the highest densities when the layer structure is fully developed. Campbell (1986*b*) was able to directly relate these observations to the microstructure development.

This material exhibits all of the possible states of granular flow. At the base, the bed is packed too tightly to permit a shearing motion and consequently exhibits solid behaviour. It then goes through the layered region in which the particles move together as a unit experiencing long-duration, sliding contacts with their neighbours.

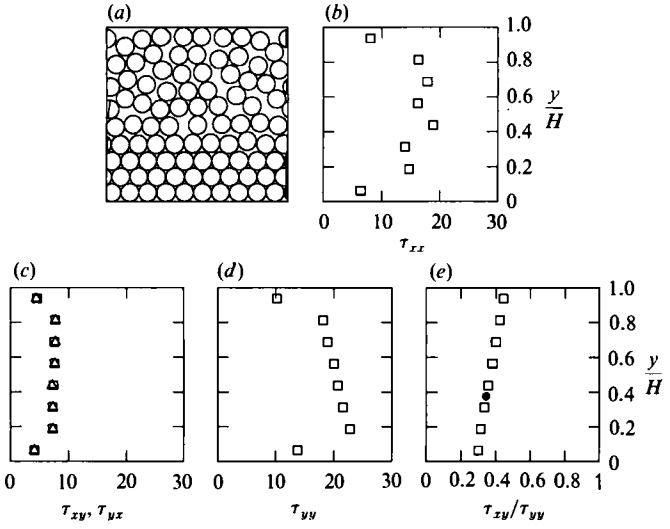

FIGURE 4. The distribution of the stress tensor components: (*b*) τ_{xx}; (*c*) τ_{xy} (□), τ_{yx} (△); (*d*) τ_{yy}; and (*e*) the stress ratio, τ_{xy}/τ_{yy}, across the control volume. Data taken from the same simulation as figures 2 and 3. A small dot has been placed on the τ_{xy}/τ_{yy} plot to indicate approximately where yielding occurs in figure 2.

The conditions here correspond to the quasi-static regime of granular flow. Finally, at the highest regions of the control volume, the particles move independently of one another in a random manner akin to the thermal motions of molecules – the behaviour associated with the rapid flow of granular materials. Surprisingly, all of these changes take place over distances of a very few particle diameters.

The internal stress distributions are shown in figure 4. The figure shows the distribution across the sample of the four components of a two-dimensional stress tensor, τ_{xx}, τ_{xy}, τ_{yx}, τ_{yy}, and the stress ratio, τ_{xy}/τ_{yy} (which is the effective friction coefficient experienced by the material). The absolute values of all components are plotted, but in all cases the normal stresses τ_{xx} and τ_{yy} are negative and the shear stresses τ_{xy} and τ_{yx} are positive. As mentioned before, the complete stress tensor $\boldsymbol{\tau}$ in each strip is the sum of the streaming stress tensor $\boldsymbol{\tau}_s$ and the collisional stress tensor $\boldsymbol{\tau}_c$. However, in all these simulations, the solid fraction is relatively high so that the streaming stress contributions are small compared to the collisional contributions. In the regions with the smallest solid fractions (near the upper wall), the streaming stresses are only 5% of the collisional stresses, and within the stagnant region, the streaming stresses are less than 1% of the collisional stresses.

As mentioned previously, τ_{xy} should be uniform across the control volume and is determined by the value applied at the top wall. At the same time, τ_{yy} increases nearly linearly from the value applied at the top wall owing to the increasing hydrostatic overburden of material. The smaller values in both components right next to the two walls appear because impulses transmitted during particle–wall collisions are not taken into account in the collisional stress calculations so that not all of the momentum transport in those strips is accounted for; we did not bother to add correction terms for these quantities, as Campbell (1988, 1992) did, as we are not interested in what happens at the walls. The stresses τ_{xx} and τ_{yx} cannot be applied by the boundaries in the current flow configuration; hence, these stresses are self-equilibrated and the values are completely determined by the flow conditions. (It

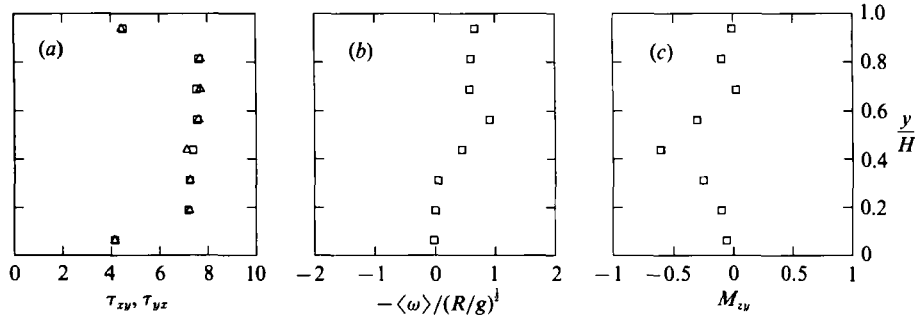

FIGURE 5. (*a*) An expanded view of the τ_{xy} (□) and τ_{yx} (△) plot from figure 4(*c*), showing asymmetry in the stress tensor, and the corresponding rotational velocity (*b*) and couple stress (*c*) distributions. Data were taken from the same simulation as figures 2, 3 and 4.

may seem that τ_{xx} is randomly distributed about a mean value, but note that it reaches its maximum value at just about the point of the effective phase change; this is consistent with most of the other data we have seen which show a local maximum there. One may speculate that this is due to the enhanced transport of x-direction force across the interlayer contact lines in that first sliding layer.) The stress ratio τ_{xy}/τ_{yy} decreases from the top to the bottom because τ_{xy} is constant while τ_{yy} increases hydrostatically with depth. While, owing to the large vertical spacing of the points, it is difficult to pinpoint exactly the stress ratio at the flowing and non-flowing transition, it appears to occur at a value of $\tau_{xy}/\tau_{yy} \approx 0.34$. (A small black circular marker has been added to this plot at the approximate point of yield within the material.) Note that in the fluidized region, τ_{xy}/τ_{yy} is greater than 0.34 and in the stagnant region, τ_{xy}/τ_{yy} is less than 0.34. This is a very small stress ratio, especially when compared to the values found by Campbell & Gong (1986) for uniformly shearing granular flows (which were typically about 0.6 for $\epsilon = 0.8$); this may indicate that the reduction in the stress ratio that Campbell & Brennen (1985) associated with the layered microstructure development, makes its effect felt throughout the entire flow field. Indeed, Campbell & Gong's uniformly shearing values are larger even than the largest stress ratio the material experiences in the current simulations (which is that applied at the top wall and, for this case, is equal to 0.47).

Figure 5 is an expanded plot of the τ_{xy} and τ_{yx} stress shown in figure 4, plotted along with the corresponding couple stress tensor component M_{zy} and the rotational velocity distribution, $-\omega/(R/g)^{\frac{1}{2}}$. These are included to show a similar type of disturbance in the couple stresses as was seen near solid boundaries by Campbell (1988, 1992). Notice that where the large rotations are observed, asymmetries appear in the stress tensor and, with them, non-zero values of the couple stress tensor. Furthermore, notice that, just above the stagnant zone, $\tau_{xy} > \tau_{yx}$ (implying a clockwise torque on the particles), in the next layer up, the two are about equal, and still one further layer up, the situation is reversed and $\tau_{yx} > \tau_{xy}$ (implying a counterclockwise torque). But also notice that these three cases nearly correspond to an increasing rotation rate, the maximum rotation rate, and a decreasing rotation rate. Now, remember from equation (7) that, under steady conditions, stress tensor asymmetries can be balanced by gradients in the couple stress tensor and the reader can qualitatively see in the data shown in figure 5, how these ideas are valid. However, the largest asymmetries occur when the gradient of the couple stress changes sign so that no quantitative evaluation is possible.

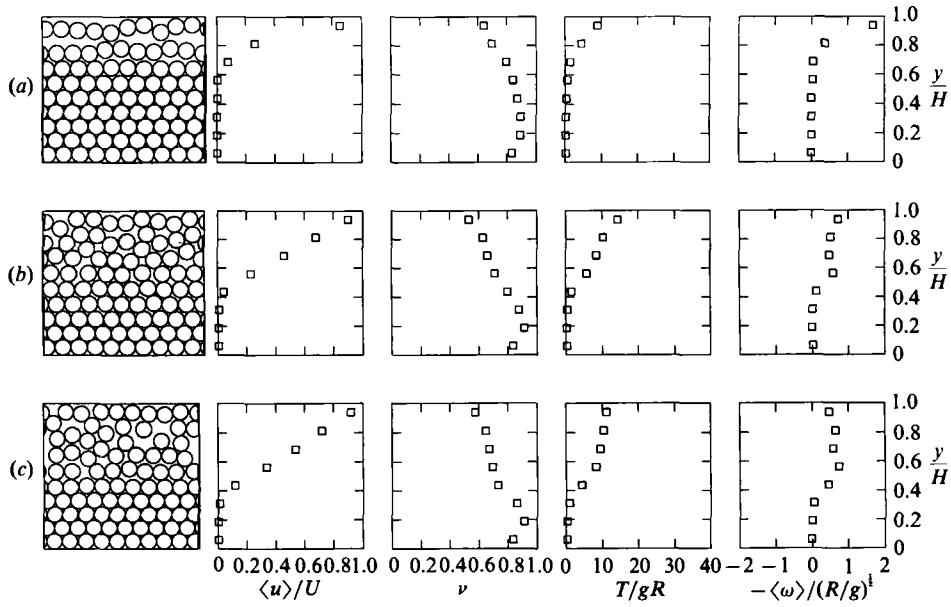

FIGURE 6. The effect of varying the applied wall shear stress, X: (*a*) $XR^2/mg = 3$ $(U/(gR)^{\frac{1}{2}} = 3.9)$, (*b*) $XR^2/mg = 3.50$ $(U/(gR)^{\frac{1}{2}} = 11.1)$, and (*c*) $XR^2/mg = 3.75$ $(U/(gR)^{\frac{1}{2}} = 14.5)$. $YR^2/mg = 7.5$, $KR/mg = 5 \times 10^5$, $\epsilon = 0.8$ and $\mu = 0.5$.

Figure 6 shows three cases with different top-wall shear forces: $XR^2/mg = 3$, 3.5, and 3.75. The normal force (or top-wall weight) and the material properties are unchanged ($YR^2/mg = 7.5$, $\epsilon = 0.8$, $\mu = 0.5$ and $KR/mg = 5 \times 10^5$). The transition region shifts towards the bottom as X increases; in other words, the larger the shear force X, the more material that is fluidized. From one point of view, increasing the shear force on the top plate increases the work performed on the material, which in turn increases the kinetic energy of the material and allows more to be fluidized. That idea supports the notion that the transition is determined by some sort of P–V–T criterion as for a normal thermodynamic material – the behaviour that one would expect from a strict interpretation of kinetic theory models of rapidly shearing granular flows. However, close examination reveals that this is not a true picture of the transition. Increasing the shear stress causes the location of the interface to move downward in the control volume so that the transition occurs at increasingly larger overburden pressures. From a kinetic theory point of view, one would expect that the increase in pressure would be balanced by an increase in either, or both, of the solid fraction and granular temperature. But here, one can see that the concentration of the transition plane is fixed at about $\nu = 0.78$, the value that corresponds to the layered microstructure. Thus, the concentration is determined solely by the structure and not by the applied forces. Furthermore, the particles on the transition plane are in contact for long periods with their neighbours and, in a granular system, pressure may be supported across those contacts with no corresponding increase in the granular temperature. In the kinetic theory picture, such as the model proposed by Jenkins & Askari (1991), particles are prohibited from experiencing long-duration contact and, at constant ν, an increased pressure could only be resisted by an increased granular temperature. That is, apparently, not the case here. Not only is there no apparent increase in the granular temperature, but it is clear from the structure in the immediate neighbourhood of the interface, that they are undergoing

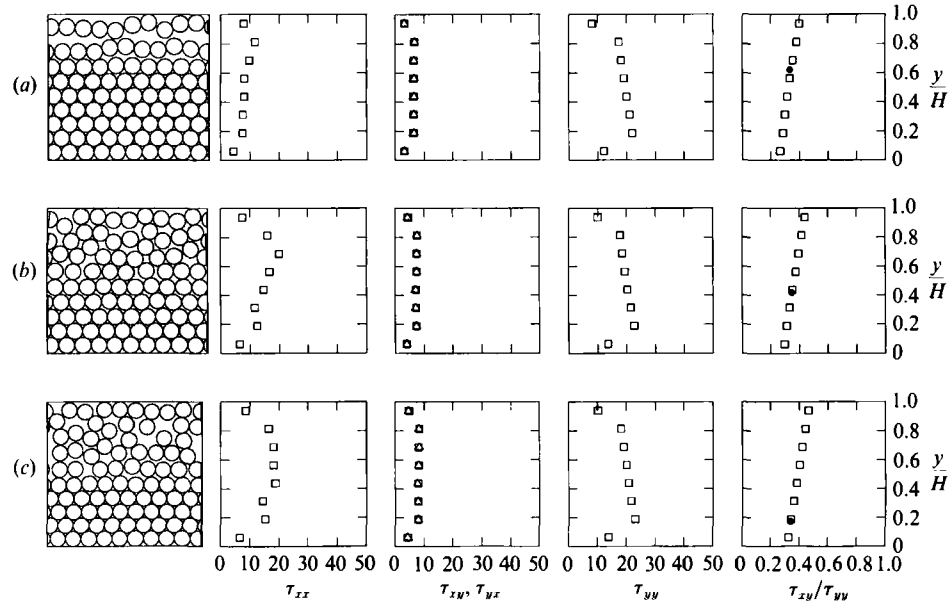

FIGURE 7. The stress distributions corresponding to figure 6. A small dot has been placed on the τ_{xy}/τ_{yy} plot to indicate approximately where yielding occurs in figure 6. In the central column □ denotes τ_{xy} and △, τ_{yx}.

long-duration contact with their neighbours. Thus, some other mechanism must account for the transition from fluid-like to solid-like behaviour.

The key to the problem can be seen in figure 7, which shows the corresponding stress distribution through the material. The most important thing to notice in this figure – which is possibly the most important finding in this paper – is that the stress ratio at the point of yielding is about the same, $\tau_{xy}/\tau_{yy} = 0.34$, in all three cases. (To keep the reader from flipping between figures 6 and 7, a small black circular marker has been placed through the point on each of the τ_{xy}/τ_{yy} plots in figure 7 that corresponds approximately to the point where yielding is apparent in the velocity profile of figure 6.) Thus, despite any arguments that can be made about energetics, it appears that the initial yield is governed only by stress considerations. In other words, the first appearance of fluidized behaviour will occur at a constant stress ratio, obeying some sort of Mohr–Coulomb failure criterion. This should have been expected as the evidence indicates that the initial failure occurs primarily as a sliding contact which is characteristic of quasi-static deformation.

This leads to an entirely different picture of what is happening in figures 6 and 7. Increasing the applied shear force is equivalent to increasing the shear stress τ_{xy} within the granular material. But, as the normal stresses τ_{yy} are the same, increasing τ_{xy} increases the stress ratio, τ_{xy}/τ_{yy}, at the top wall. As mentioned previously, the stress ratio decreases as one moves downward through the material since τ_{xy} is constant, but τ_{yy} increases with depth, owing to the increasing overburden of material. Hence, as the top-wall shear force is increased, the location where the stress ratio falls to its critical value of about 0.34 occurs progressively deeper within the material and, consequently, more of the material is fluidized. But one cannot say that the energetics have nothing to do with the phase change. For example, it is clear from examining the temperature profile in figure 6 that the larger the wall shear

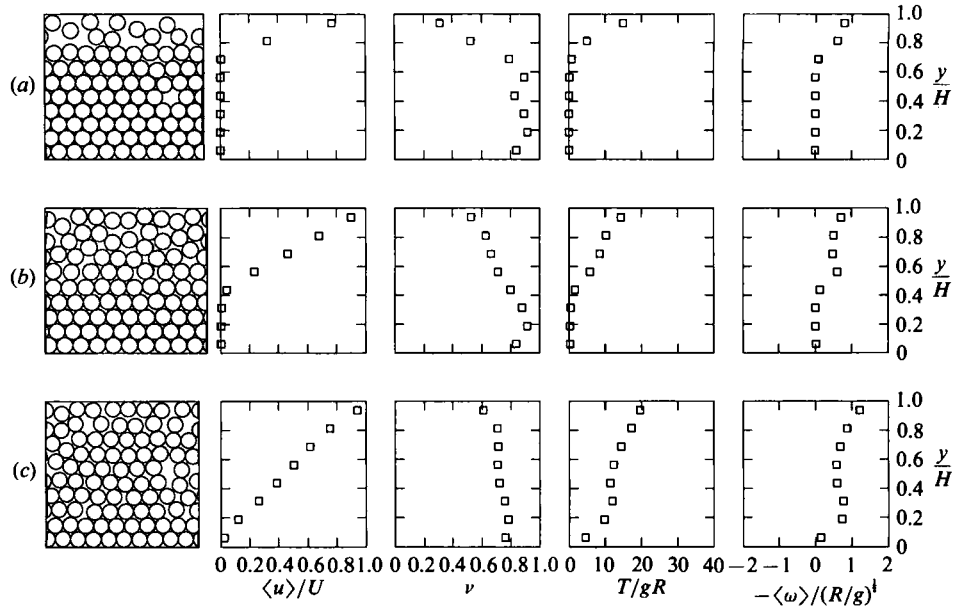

FIGURE 8. The effect of varying the applied normal stress, Y, while keeping the applied stress ratio fixed at $X/Y = 0.47$: (*a*) $YR^2/mg = 2.5$ $(U/(gR)^{\frac{1}{2}} = 5.1)$, (*b*) $YR^2/mg = 7.5$ $(U/(gR)^{\frac{1}{2}} = 11.1)$, and (*c*) $YR^2/mg = 15$ $(U/(gR)^{\frac{1}{2}} = 27.1)$. $KR/mg = 5 \times 10^5$, $\epsilon = 0.8$ and $\mu = 0.5$.

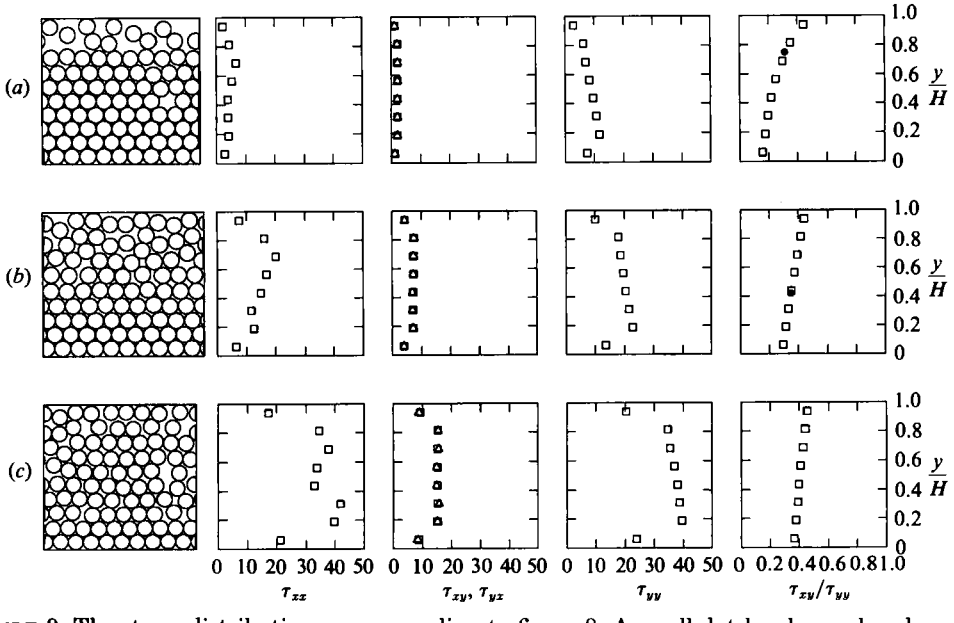

FIGURE 9. The stress distributions corresponding to figure 8. A small dot has been placed on the τ_{xy}/τ_{yy} plot to indicate approximately where yielding occurs in figure 8. In the central column, □ denotes τ_{xy} and △, τ_{yx}.

force, X, the more random kinetic energy is contained in the flow (which simply reflects the larger shear work performed at the wall.) Thus, it seems there are two separate processes that, together determine the transition to a fluidized state. First, the initial failure may well be determined by a Coulomb failure criterion. But that

does not in itself describe the nature of the flow field. For example, if the stress ratio were the sole criterion, a possible solution would be two, essentially solid, blocks slipping relative to one another along a thin shear zone that is the order of a partical diameter thick. In the current simulations, the overburden relaxes sufficiently while moving upward in the control volume to permit the material to assume rapid flow behaviour. Such would not be the case if the applied normal force were significantly larger than the hydrostatic pressure variation across the control volume. Thus, while a stress-ratio condition controls the transition from solid to quasi-static behaviour, the final transition from quasi-static to rapid flow depends on other criteria.

To see the effect of normal stress τ_{yy} on the fluidization, figures 8 and 9 show three cases for which the normal force, Y, applied externally on the upper wall is changed while the ratios of the external shear force and normal force is held fixed at $X/Y = 0.47$. (In all cases, $\epsilon = 0.8$, $\mu = 0.5$ and $KR/mg = 5 \times 10^5$.) In other words, the stress ratio, τ_{xy}/τ_{yy}, at the upper wall does not change, despite changing τ_{yy}. (Note that this may also be interpreted as changing τ_{xy} with the stress ratio held constant.) The plots indicate that the larger the value of τ_{yy}, the more material that is maintained in a fluidized state. This is contrary to what one would expect if the analogy between a rapid granular flow and molecules in the kinetic theory is taken too strongly. In a molecular system, one would expect that the larger the pressure, the more likely the system would be to experience solid behaviour. But also, in a thermodynamic system the temperature can be set independently by bringing the system into contact with an isothermal reservoir, while in a granular material the temperature depends on the flow conditions, and this difference permits such unexpected behaviour. Why the fluidized region grows as the normal stress increases may be understood by first noting that the larger the normal stress, τ_{yy}, the larger the dispersive stresses that must be generated within the fluidized material. As the dispersive stresses maintain the material in a fluidized state, the larger the dispersive stresses the more material that is fluidized. These arguments can explain the level of activity in the fluidized region but cannot explain the location of the fluid/solid interface. That explanation can only be made using stress ratio arguments. Note that the larger the normal stress at the top wall, the smaller the fractional change that the overburden of material can cause in τ_{yy} between the top and bottom of the channel. Thus, if the stress ratio, τ_{xy}/τ_{yy}, is held fixed at the top of the channel, the larger the value of τ_{yy} the less the stress ratio drops across the channel and the deeper the point at which the yield stress ratio (about 0.34) is reached. Note that these results indicate that stagnant zones are more likely to form under conditions of small stress loadings. In this way, they are consistent with the observations made by Nguyen (1979) and Nguyen, Brennen & Sabersky (1980) that flow in hoppers will change from a fully fluidized state to funnel flow as they are emptied. In the light of the current findings, as Nguyen's hoppers are emptied, the normal stresses are reduced, making the material harder to fluidize, and the stagnant regions that form the funnel appear.

There is an interesting sidenote worth mentioning here. For almost all of these studies, the solid layer is packed into a perfect crystalline structure with the particles arranged in a hexagonal close packed configuration. However, for $YR^2/mg = 2.5$, there is a defect in the stagnant region. Particles on the top of the vacancy are arched over it and support the rest of particles above them. This arch is not observed in any other cases and exists here probably because of the small stress state. One way to look at the situation is that the arch can only support a certain amount of force and only the low stresses present in this case are within this limit, while stresses in all the other cases exceed it. But the real explanation is probably a bit more complicated.

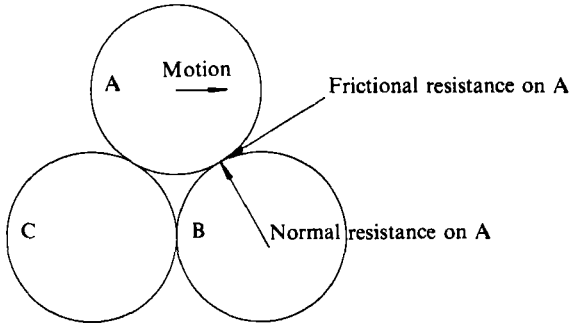

FIGURE 10. A schematic of particle interaction near the transition interface.

As mentioned in the last paragraph, the larger the dispersive stresses the larger the granular temperature. If enough granular temperature can be conducted into the area surrounding the arch, it would cause variations in the instantaneous normal stresses supported across the contact point and may even cause a momentary loss of contact between particles. This could greatly weaken the frictional bonds and cause the arch to collapse. It is worth mentioning at this point that none of the cases here were started with the particle centres arranged in the triangular configuration we have found to be characteristic of the solid-like regions of the material. Instead, a combination of the stress state and the particle activity have forced the system to assume this state through a process not unlike the settling of a cup of flour by a series of gentle taps.

What remains to be done is to try and determine the effect of the particle properties, the stiffness coefficient, K, the friction coefficient, μ and the coefficient of restitution, ϵ (or alternatively the damping coefficient D) on the yield properties of the granular mass. The effect of material properties on the transition process is easier to understand if considered in the light of figure 10 which shows three particles locked in a triangular packing. The reader should imagine that particle A is a member of a layer trying to move to the right over another layer containing particles B and C. The motion is resisted by a combination of tangential and normal forces generated across the contact point with particle B. The tangential forces, which are related to the particle surface friction coefficient, μ, resist sliding between the two surfaces and will cause particle A to roll – unless the rolling is prevented by further interactions between particle A and other particles in the granular mass. The normal resistance, which will be related to the particle stiffness coefficient, K, forces particle A to move upward over particle B in order to pass by unless such movement is likewise resisted by other particles. The dependence on the coefficient of restitution is more indirect but hopefully will become clear in the following discussion.

The effect of the coefficient of restitution, ϵ, is illustrated in figure 11 with the corresponding stress information plotted in figure 12. (For each, $XR^2/mg = 3.5$, $YR^2/mg = 7.5$, $\mu = 0.5$ and $KR/mg = 5 \times 10^5$.) Four cases are pictured, corresponding to $\epsilon = 0.4$, 0.9, 0.95 and 0.98. Apparently, below $\epsilon = 0.9$, the results are nearly independent of ϵ (compare the figures for $\epsilon = 0.4$ and 0.9) and the value of ϵ only becomes important very near $\epsilon = 1.0$. This is a rather surprising result: since the coefficient of restitution governs the rate of energy dissipation within the material, one would expect a very strong dependence on ϵ. The smaller ϵ, the larger the energy dissipation and the smaller one would expect the granular temperatures. Yet, as the magnitudes of the granular temperatures are roughly the same at $\epsilon = 0.4$ as at

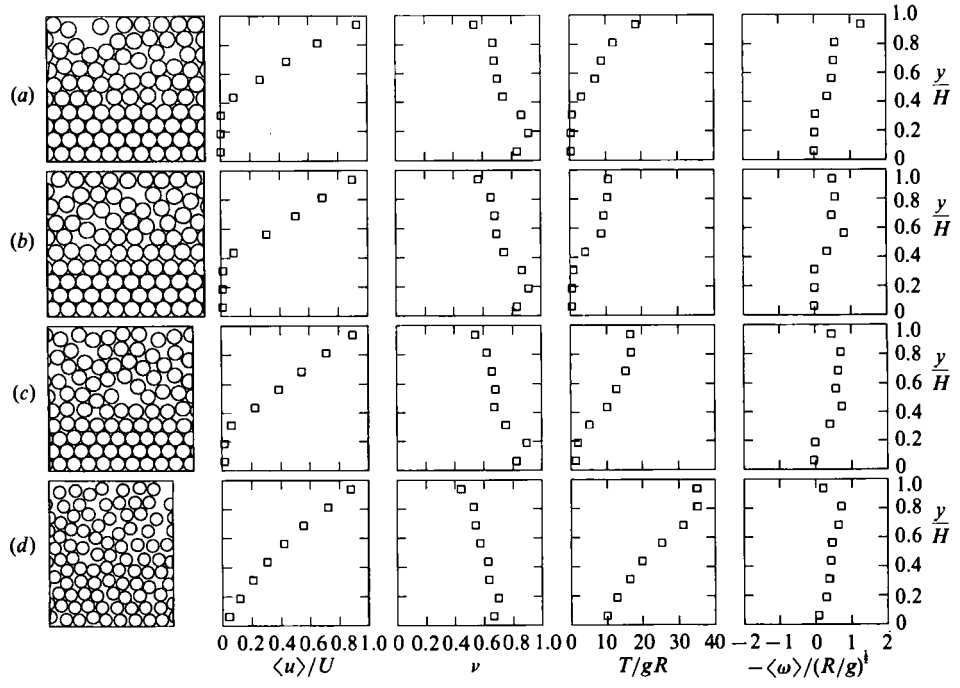

FIGURE 11. The effect of varying the coefficient of restitution, ϵ: (*a*) $\epsilon = 0.4$ $(U/(gR)^{\frac{1}{2}} = 12.3)$, (*b*) $\epsilon = 0.9$ $(U/(gR)^{\frac{1}{2}} = 13.4)$, (*c*) $\epsilon = 0.95$ $(U/(gR)^{\frac{1}{2}} = 17.6)$ and (*d*) $\epsilon = 0.98$ $(U/(gR)^{\frac{1}{2}} = 23.6)$. $XR^2/mg = 3.5$, $YR^2/mg = 7.5$, $KR/mg = 5 \times 10^5$ and $\mu = 0.5$.

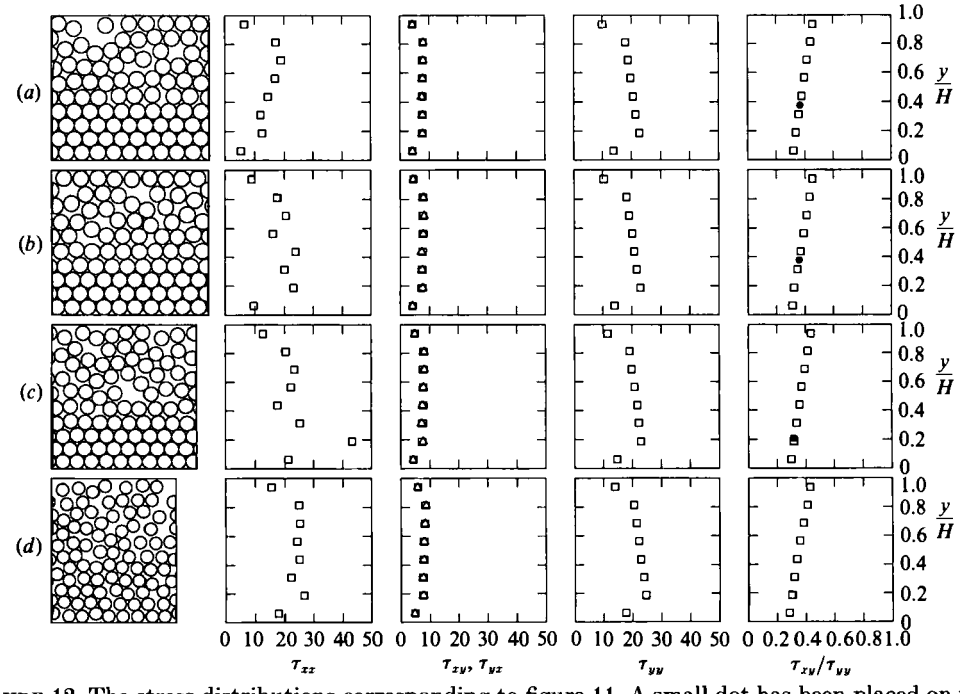

FIGURE 12. The stress distributions corresponding to figure 11. A small dot has been placed on the τ_{xy}/τ_{yy} plot to indicate approximately where yielding occurs in figure 11. In the central column, □ denotes τ_{xy} and △, τ_{yx}.

$\epsilon = 0.9$, this is clearly not the case. This behaviour can be understood by examining the unscaled data which show that the top-wall velocity is about 10% greater for $\epsilon = 0.4$ than for $\epsilon = 0.9$, indicating that the top wall does about 10% more work or, alternatively, that there is about 10% more energy dissipation with the $\epsilon = 0.4$ material. Further evidence can be obtained by examining the temperature profile, which shows much more uniform temperatures for $\epsilon = 0.9$ than for $\epsilon = 0.4$; the temperature gradient throughout the fluidized region for the $\epsilon = 0.4$ case (which implies large conduction of granular temperature), reflects the greater energy dissipation within the material and the greater need to conduct energy from the top wall to keep the interior of the fluidized region active. Note that these results are, once again, inconsistent with the kinetic theory based model of Jenkins & Askari (1991) which predicts the stress ratio at transition should vary as $(1-\epsilon)^{\frac{1}{2}}$.

Despite these rather trivial differences, changing the restitution coefficient from $\epsilon = 0.4$ to 0.9 apparently has no effect on the transition from fluid to solid behaviour. The velocity and density profiles are nearly identical and, consequently, so are the stress distributions. But this should be expected as the initial failure is governed by quasi-static behaviour which should be independent of the energetics of the rapid flow region. However, at $\epsilon = 0.95$, progressively more of the material is fluidized and at $\epsilon = 0.98$, the whole material is behaving as a fluid. (The change in control volume shape for the larger coefficients of restitution is due to the increased height as the top wall is lifted up by the highly energetic particles.) Yield occurs at about $\tau_{xy}/\tau_{yy} = 0.34$ for $\epsilon \leqslant 0.9$ and at about $\tau_{xy}/\tau_{yy} = 0.325$ for $\epsilon = 0.95$; no judgment can be made from figure 12 for the $\epsilon = 0.98$ case as the entire material shears; however, an additional simulation, run with different stress conditions, indicates that the yield stress ratio is about $\tau_{xy}/\tau_{yy} \approx 0.27$. It is not completely clear what makes these two cases different from all those in the range $0.4 \leqslant \epsilon \leqslant 0.9$, but we can speculate on the reasons. Note that the granular temperature just inside the border of the solid region of the $\epsilon = 0.9$ plot is only marginally larger than that of the $\epsilon = 0.4$ plot, but the corresponding value is much larger for $\epsilon = 0.95$, indicating a larger degree of activity in the particles immediately surrounding the yielding layer. Referring to figure 10, a vibration of particle A causes the contacts with particle B to become intermittent; naturally, when the contacts are broken, both the tangential and normal contact forces disappear so that the effect of vibration is to reduce the effective frictional reaction between the layers. Apparently, for $\epsilon \leqslant 0.9$ the granular temperature is damped to such a degree that it cannot significantly aid the yield process by the time it reaches the first moving layer; thus, an effect will only be felt for the largest coefficients of restitution. Note that $\epsilon = 0.95$ and 0.98 are the only cases for which it can be argued that the behaviour in the rapid flow regime has any effect on the quasi-static yield process.

The effect of particle friction coefficient on the transition is shown in figures 13 and 14. (In all cases, $XR^2/mg = 3.5$, $YR^2/mg = 7.5$, $\epsilon = 0.8$ and $KR/mg = 5 \times 10^5$.) Decreasing the particle friction coefficient increases the depth of the flowing region. The effect is small, but noticeable, between $\mu = 0.5$ and 0.2; however, when μ is reduced to zero, there is no solid region and the entire material shears. The stress ratio at yield was again $\tau_{xy}/\tau_{yy} = 0.34$ for $\mu = 0.5$, falling to 0.32 for $\mu = 0.2$. As the entire material is shearing, no information about the yield stress for $\mu = 0$ can be derived for the case shown here; however, an additional simulation, run with different stress conditions, revealed the yield stress ratio for $\mu = 0$ to be about 0.28. Thus, as might be expected, the smaller μ, the weaker the material. This can be understood by remembering that the initial failure occurs as the motion of an entire

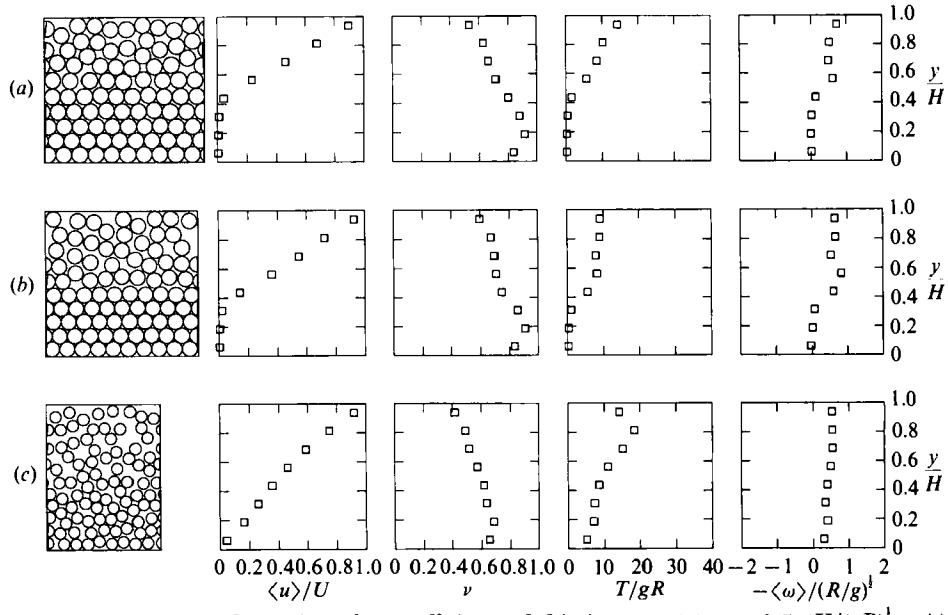

FIGURE 13. The effect of varying the coefficient of friction, μ: (*a*) $\mu = 0.5$ $(U/(gR)^{\frac{1}{2}} = 11.1)$, (*b*) $\mu = 0.2$ $(U/(gR)^{\frac{1}{2}} = 17.3)$ and (*c*) $\mu = 0$ $(U/(gR)^{\frac{1}{2}} = 42.5)$. $XR^2/mg = 3.5$, $YR^2/mg = 7.5$, $KR/mg = 5 \times 10^5$ and $\epsilon = 0.8$.

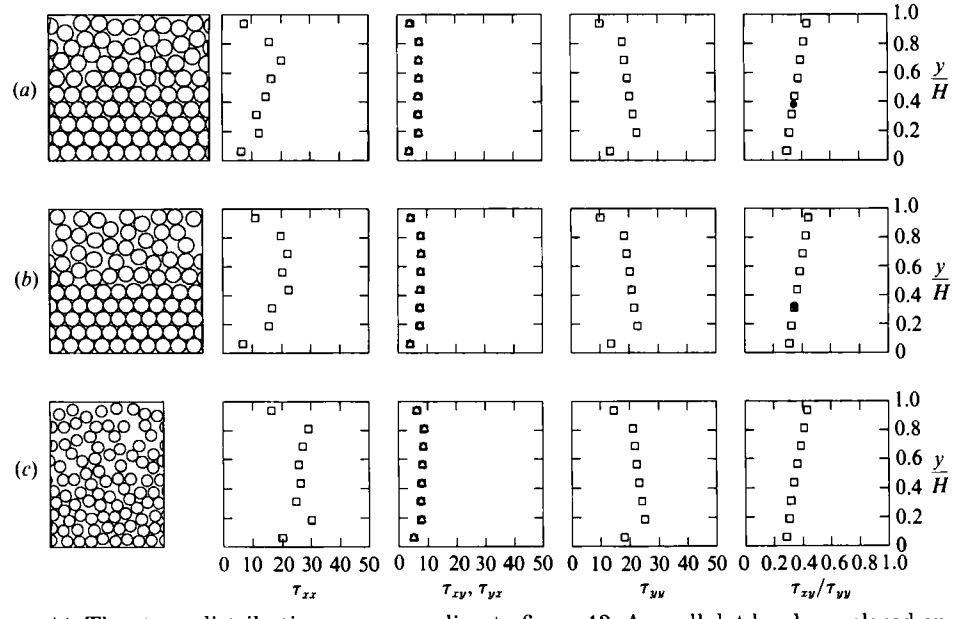

FIGURE 14. The stress distributions corresponding to figure 13. A small dot has been placed on the τ_{xy}/τ_{yy} plot to indicate approximately where yielding occurs in figure 13. In the central column, □ denotes τ_{xy} and △, τ_{yx}.

layer of particles and, within that layer, the frictional interaction between a particle and its neighbours within the layer tends to keep the particles from rotating. Hence, the failure occurs with the layer of particles sliding over the stagnant layer below it and, obviously, the interparticle friction forces will play a large part in resisting that

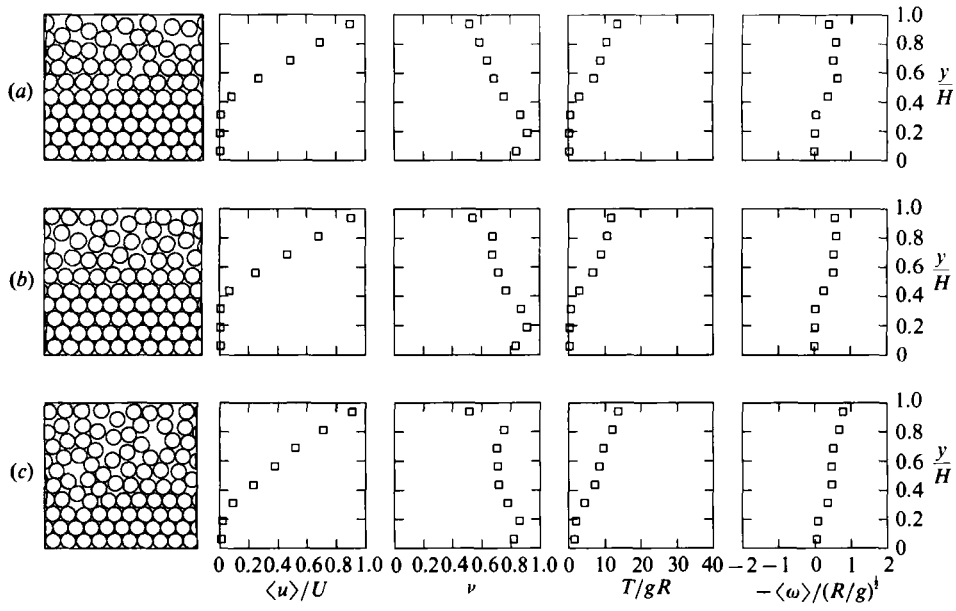

FIGURE 15. The effect of varying the stiffness coefficient, K: (*a*) $KR/mg = 5\times10^5$ $(U/(gR)^{\frac{1}{2}} = 12.9)$, (*b*) $KR/mg = 5\times10^5$ $(U/(gR)^{\frac{1}{2}} = 11.7)$, and (*c*) $KR/mg = 5\times10^5$ $(U/(gR)^{\frac{1}{2}} = 11.1)$. $XR^2/mg = 3.5$, $YR^2/mg = 7.5$, $\epsilon = 0.8$ and $\mu = 0.5$.

motion (although it should not be forgotten that, as shown in figure 10, forces normal to the point of contact also add to the material's strength). Consequently, the smaller the interparticle friction coefficient, the easier it is to set a layer of particles in motion. Note that, surprisingly, the stress ratio at yield can be smaller than the particle surface friction coefficient.

We also observed that for $\mu > 0.6$ the whole system seems unstable. Then, because particles cannot slip easily with respect to one another, large, strong clusters of particles, with essentially solid behaviour, are frequently formed. Sometimes, a cluster is long enough to form a column that spans from the upper to the lower wall and acts as a pole on which all of the force applied at the upper wall is supported. This has two effects. First, the top wall is lifted up on the pole causing an increase in the depth of the control volume. This is not surprising and a similar scenario has been used to explain large-scale oscillations in the wall separation and stresses observed in granular shear cell testers (see, for example, Savage & Sayed 1984). While the top wall is being lifted, a tremendous amount of energy is stored in the potential energy of the bonds. Consequently, as the cluster breaks, the potential energy is transferred into kinetic energy, throwing the whole system into a state of chaos. After a while, the system settles down to the previous state until a new column is formed and the same procedure is repeated. The practical upshot of all this is that this configuration is unsuitable for studying systems with large friction coefficients because the results become sensitive to the spacing of the solid walls. However, our observations indicate that there is no additional understanding to be gained by studying systems with larger μ.

The effect of the third material property, the particle stiffness coefficient, K, is shown in figures 15 and 16, for the velocity and stress data respectively. Plots

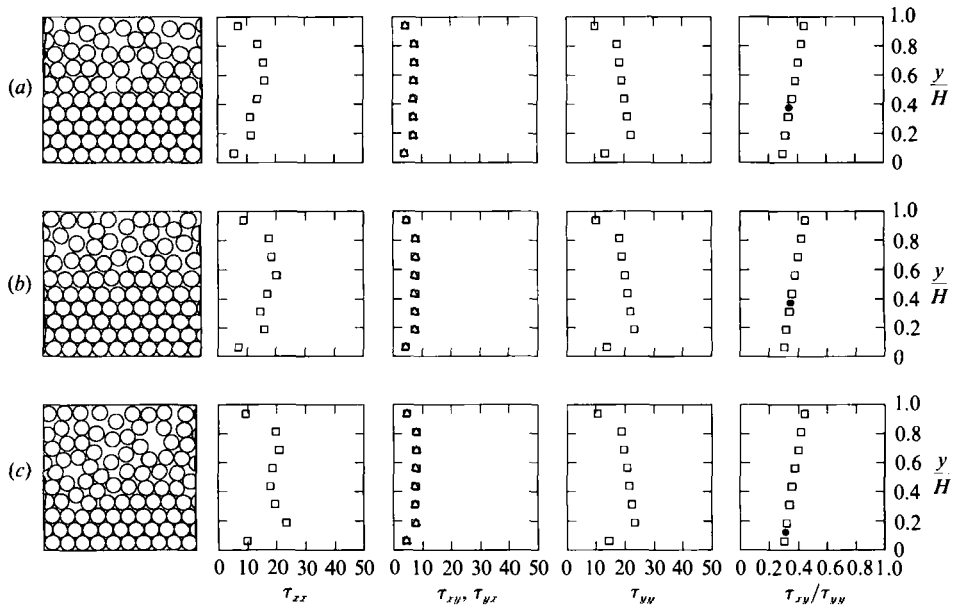

FIGURE 16. The stress distributions corresponding to figure 15. A small dot has been placed on the τ_{xy}/τ_{yy} plot to indicate approximately where yielding occurs in figure 15.

are shown for $KR/mg = 5\times10^3$, 5×10^4 and 5×10^6. In all cases, $XR^2/mg = 3.5$, $YR^2/mg = 7.5$, $\epsilon = 0.8$ and $\mu = 0.5$. Although, again, the results show very little effect of changing K until it falls to very small values, these observations do yield some insight into the transition process. Somewhat surprisingly, the results indicate that very soft particles fluidize more readily than hard ones. For $KR/mg = 5\times10^4$ and 5×10^6, the yield occurs at a stress ratio of $\tau_{xy}/\tau_{yy} = 0.34$ (the same as before), but for $KR/mg = 5\times10^3$, this value has fallen to $\tau_{xy}/\tau_{yy} = 0.30$. (An additional case was run for $KR/mg = 500$, but the entire mass sheared so that the yield stress ratio could not be determined.) This may be beter understood by recalling the yield process illustrated in figure 10. Applying a loading to the particles in that configuration will cause the particles to overlap as a reaction to the normal force applied to the point of contact. But notice that only a small portion of particle B resists the motion of particle A to the left, and, if the particles are soft enough, particle A may pass through the barrier provided by particle B. This is apparently what is occurring in the cases shown in figures 15 and 16. But notice that the particles have to be extremely soft before any effect of the stiffness is apparent in the yield behaviour.

Collectively, these results illustrate that the yielding behaviour is relatively insensitive to material properties as changes were only observed in extreme cases of large ϵ and of small K and μ.

4. Conclusions

This paper describes a study of the effective phase transition between fluid and solid behaviour that is all too common in devices that handle granular materials. The results show that such an interface encompasses the entire range of granular flows, from stagnant elastic solid-like material, to quasi-static behaviour where the

deformation occurs with long-duration contacts between particles, to fully fluidized rapid granular flows where the particles move independently of one another in a manner analogous to the motion of molecules in the kinetic theory of gases. And all of this takes place over a range of only a few particle diameters.

The most important result of this paper is that the point where yield is initially observed seems to be determined solely by the stress ratio, τ_{xy}/τ_{yy}, which is, in turn, a function only of the particle properties. This indicates that the interface between fluid and solid behaviour can be governed by a Mohr–Coulomb failure criterion, which should be expected because the initial yield occurs when the material is exhibiting quasi-static behaviour where such criteria have long been known to apply. But such a failure criterion only defines the location of the interface between the moving and stationary regions and does not, in itself, describe the radical change that occurs between solid behaviour and 'free molecular' rapid granular flow only a few particle diameters away. However, it is clear that the currently popular analogy between granular and real thermodynamic materials is carried too far and that the 'phase-change' is not described by a P–V–T type criterion, based on the granular temperature, such as has been recently proposed by Jenkins & Askari (1991). Interestingly, the fully fluidized region above the interface appears to have very little effect on the yield at the interface. Interplay between the two was only observed for the most extreme values of the coefficient of restitution ($\epsilon \geqslant 0.95$), where the granular temperature at the interface was large enough to presumably cause intermittent contact between the first moving layer and the stagnant bed, thus weakening the interface. Otherwise, the yield condition appears to be unchanged by the flow conditions.

Although unexpected, for those of us that approached this problem from a rapid-flow point of view, it should not be surprising to find the transition to be a yield-like phenomenon occurring while the material is undergoing quasi-static deformation. The key lies in the results of Campbell & Gong (1986) which indicate that the stress ratios generated by a uniformly shearing rapid granular flow are larger than is required to cause quasi-static yield. Thus, it is difficult to imagine that one could have a rapid granular flow in the presence of a stagnant region *without* causing quasi-static yield within the static material. Such a case would only be possible if the nature of the phase-change interface influenced the rapid flow to the extent that it reduced the local stress ratio significantly below the value found in an undisturbed uniform shear flow. An interesting, and as yet undiscussed, byproduct of these results is that the boundary can cause just a reduction in the local stress ratio (although not a large enough reduction to pull the stress ratio below the quasi-static yield point). This is apparent in that nowhere in the results presented here are the stress ratios as large as are found in a uniformly shearing granular flow, even though there are many examples in which the flow above the interface has all of the characteristics of a uniform shear flow.

However, the picture is still not complete. If the particles on the interface slide while experiencing long-duration contact with their neighbours, it is somewhat surprising that the friction coefficient at yield is only weakly dependent on the particle surface friction; for example, in the majority of cases shown in this paper, the flow yields at $\tau_{xy}/\tau_{yy} \approx 0.34$ which is smaller than the particle surface friction coefficient, $\mu = 0.5$. It is not clear how a long-duration contact can exhibit constant yielding at a value smaller than the surface friction coefficient. This quandary led us to perform a detailed investigation of the behaviour of yielding at the interface. Figure 17 shows time traces of the x-direction velocities at various vertical

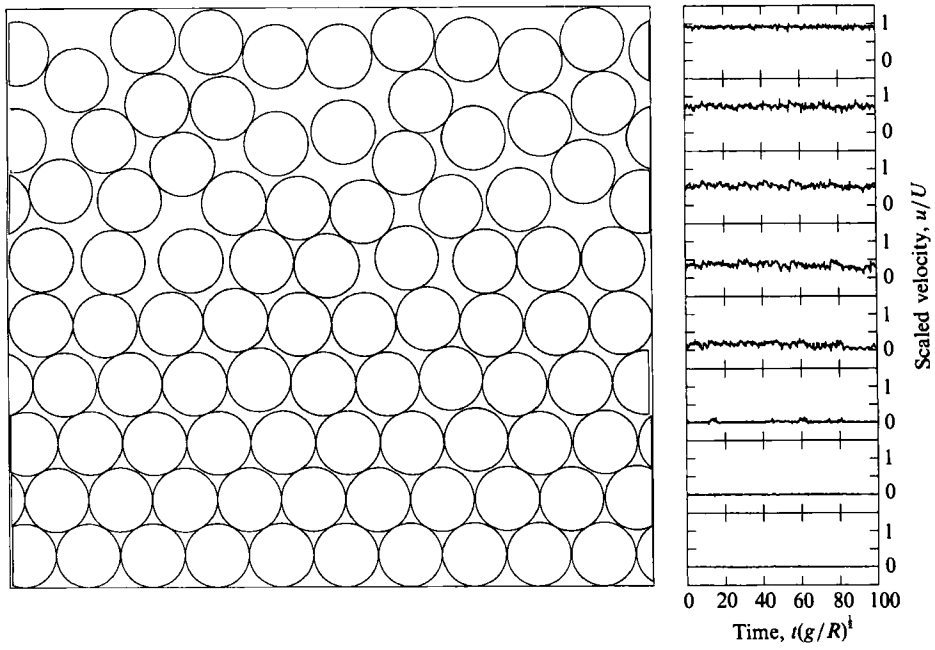

FIGURE 17. Time traces of the particle velocities at various locations across the control volume. The values shown are the average velocities of the particles that lie within the corresponding portion of the control volume.

coordinates through the control volume for the simulation shown in figures 2–5. This shows that the initial motion, which occurs in third strip up from the bottom, occurs only sporadically. Similar behaviour can be observed in the fourth strip from the bottom; there, the particles are generally in motion, although they do appear to come to a stop for short periods of time. (This is particularly apparent near the end of the time trace shown here.) Below the third strip the material does not move, and only shows slight fluctuating velocities due to the small granular temperature in that region. Above the fourth strip, the particles are in continuous motion although they too show discernible fluctuations of a much larger scale. Thus, the slip is not a continuous motion and cannot be directly related to the surface friction. It appears that the forces experienced by the layer are only sporadically large enough to force the layer to move. This allows the average stress on the interface to be somewhat smaller than would be required to induced continuous yielding.

Interestingly, a phase-change interface may be somewhat easier to handle theoretically than solid interfaces. A solid interface, such as the wall of a hopper, is described by its shape and its material properties. One knows where the boundary is, but one cannot immediately know what values the flow properties, such as the velocity, density and granular temperature, assume at that boundary as these will be governed by the conditions in the flow far away. Such a problem cannot be solved using the standard procedure of first finding the general solution and then applying known boundary conditions. Instead, the problem for the entire flow, boundary included, must be determined simultaneously. (See, for example, Jenkins & Richman 1986.) But in the effective phase-change boundary observed here, the location of the boundary is unknown, although one can very accurately assume that both the velocity and granular temperature go to zero, the density corresponds to an

unshearable packed bed state and the stress ratio is that which corresponds to initial yield. Thus, this is the reverse problem: the conditions at the boundary are known, but its location is not. However, the location can be determined solely from stress conditions and finding its position could be a very simple procedure. For example, in the Couette flow with gravity studied here, the stress conditions at the top wall are known and from that the size of material overburden required to reduce the stress ratio at the top wall to the yield value can be easily calculated. One then knows exactly how much material is fluidized so that the boundary is located at the upper surface of a packed bed formed by the unfluidized fraction of the material.

These results should hearten plasticity theorists and others who use Mohr–Coulomb type failure criteria to predict flow/no-flow situations. All of this gives strong support to theories such as that presented by Johnson & Jackson (1987), which incorporate, in an *ad hoc* manner, a Mohr–Coulomb failure criterion within the framework of a rapid granular model. However, even they might be surprised at the rapidity with which the flows studied here change from stagnant, through quasi-static to rapid flow behaviour.

The far-reaching consequence of this work is that it gives one further bit of evidence that the applicability of the rapid-flow/kinetic-theory models, that have been so popular in recent years, is limited to rapidly sheared regions of flow, such as those near boundary surfaces; in particular, they cannot model the behaviour through the transition to solid-like behaviour. This is unfortunate. The rapid granular flow models were extremely attractive as they were well grounded in the formalisms of kinetic theory, and can be used to infer the behaviour of the bulk material from the properties of individual particles. No similarly well-grounded theory exists for even the quasi-static regime, and it will be a long time before such a model can be found that spans the realm between the two regimes in a way that can accurately account for the transition from fluid-like to solid-like behaviour.

This study was supported by the International Fine Particle Research Institute, the National Science Foundation under grant number MEA-8352513, and Sun Microsystems for which the authors are extremely grateful. Thanks also to Roland Clift for sparking our minds by posing a question for which we did not have a good answer. Additional thanks are due Holly Campbell for proofreading the manuscript and to Ian and Sean for allowing her enough free time.

REFERENCES

CAMPBELL, C. S. 1982 Shear flows of granular materials. PhD thesis; Rep. E-200.7. Division of Engineering and Applied Science, California Institute of Technology, 260 pp.

CAMPBELL, C. S. 1986*a* Computer simulation of rapid granular flows. In *Proc. 10th US Natl Congr. of Applied Mechanics, Austin Texas, June 1986*, pp. 327–338. ASME.

CAMPBELL, C. S. 1986*b* The effect of microstructure development on the collisional stress tensor in a granular flow. *Acta Mech.* **63**, 61–72.

CAMPBELL, C. S. 1988 Boundary interactions for two-dimensional granular flows: asymmetric stresses and couple stresses. In *Micromechanics of Granular Materials* (ed. M. Satake & J. T. Jenkins), pp. 163–174. Elsevier.

CAMPBELL, C. S. 1989 The stress tensor for simple shear flows of a granular material. *J. Fluid Mech.* **203**, 449–473.

CAMPBELL, C. S. 1900 Rapid granular flows. *Ann. Rev. Fluid Mech.* **22**, 57–92.

CAMPBELL, C. S. 1992 Boundary interactions for two-dimensional granular flows. Part 1. The type A and type B boundary conditions. *J. Fluid Mech.* (submitted).

CAMPBELL, C. S. & BRENNEN, C. E. 1985 Computer simulation of granular shear flows. *J. Fluid Mech.* **151**, 167–188.

CAMPBELL, C. S. & GONG, A. 1986 The stress tensor in a two-dimensional granular shear flow. *J. Fluid Mech.* **164**, 107–125.

CAMPBELL, C. S. & GONG, A. 1987 Boundary conditions for two-dimensional granular flows. In *Proc. Sino-US Intl Symp. on Multiphase Flows, Hangzhou, China, August, 1987*, Volume I, pp. 278–283. Zhejiang University Press.

CAMPBELL, C. S. & ZHANG, Y. 1989 Solidification, leading to clogging in powder flows: a progress report to the international fine particle research institute. Rep. IFPRI.1, Department of Mechanical Engineering, University of Southern California, 41 pp.

JENKINS, J. T. & ASKARI, E. 1991 Boundary conditions for granular flows: phase interfaces. *J. Fluid Mech.* **223**, 497–508.

JENKINS, J. T. & RICHMAN, M. W. 1986 Boundary conditions for plane flows of smooth, nearly elastic, circular disks. *J. Fluid Mech.* **171**, 53–69.

JOHNSON, P. C. & JACKSON, R. 1987 Frictional-collisional constitutive relations for granular materials with applications to plane shearing. *J. Fluid Mech.* **176**, 67–93.

NGUYEN, T. V. 1979 Studies in the flow of granular materials. PhD thesis; Rep. E200.1, California Institute of Technology, 143 pp.

NGUYEN, T. V., BRENNEN, C. E. & SABERSKY, R. H. 1980 Funnel flow in hoppers. *Trans. ASME* E: *J. Appl. Mech.* **47**, 729–735.

SAVAGE, S. B. & JEFFREY, D. J. 1981 The stress tensor in a granular flow at high shear rates. *J. Fluid Mech.* **110**, 255–272.

SAVAGE, S. B. & SAYED, M. 1984 Stresses developed by dry cohensionless granular materials in an annular shear cell. *J. Fluid Mech.* **142**, 391–430.

WOLF, E. H. & HOHENLEITEN, H. L. VON 1945 Experimental study of the flow of coal in chutes at Riverside generating plant. *Trans. ASME* **67**, 585–599.

ZHANG, Y. & CAMPBELL, C. S. 1990 Errodable boundaries in granular flow. In *Proc. Second World Congress on Particle Technology, Kyoto, Japan, September, 1990*, Part II, 166–173.